

Experimental feedback linearisation of a non-smooth nonlinear system by the method of receptances

Mathematics and Mechanics of Solids
1–18



© The Author(s) 2018

Reprints and permissions:

sagepub.co.uk/journalsPermissions.nav

DOI: 10.1177/1081286517744601

journals.sagepub.com/home/mms



Domenico Lisitano 

Department of Management and Production Engineering, Politecnico di Torino, Torino, Italy

Shakir Jiffri

School of Engineering, University of Liverpool, Liverpool, UK

Elvio Bonisoli

Department of Mechanical and Aerospace Engineering, Politecnico di Torino, Torino, Italy

John E Mottershead

School of Engineering, University of Liverpool, Liverpool, UK

Received 11 August 2017; accepted 31 October 2017

Abstract

Input–output partial feedback linearisation is experimentally implemented on a non-smooth nonlinear system without the necessity of a conventional system matrix model for the first time. The experimental rig consists of three lumped masses connected and supported by springs with low damping. The input and output are at the first degree of freedom with a non-smooth clearance-type nonlinearity at the third degree of freedom. Feedback linearisation has the effect of separating the system into two parts: one linear and controllable and the other nonlinear and uncontrollable. When control is applied to the former, the latter must be shown to be stable if the complete system is to be stable with the desired dynamic behaviour.

Keywords

Active vibration control, receptance method, non-smooth nonlinearity, feedback linearisation

1. Introduction

The classical feedback linearisation method, well-known through text books such as [1–3], requires the use of a numerical model of the system. It is generally applicable to under-actuated systems and, by an application of a linear transformation, the system is separated into two parts. An artificial input is applied to the first part that renders it linear and enables classical linear control methods, such as pole placement, to be applied. The second part generally remains nonlinear and is rendered uncontrollable by the transformation. The stability of the second part is guaranteed when the zero dynamics (i.e. the

Corresponding author:

John E Mottershead, School of Engineering, University of Liverpool, Liverpool L69 3GH, UK.

Email: j.e.mottershead@liverpool.ac.uk

second part with the controlled coordinates set to zero and subject to arbitrary disturbance) are stable. The method of receptances is an active control method that makes use of measurements acquired directly from the test structure and therefore eliminates the necessity of evaluating the system mass, damping and stiffness matrices \mathbf{M} , \mathbf{C} , \mathbf{K} . The receptance method was introduced for single-input systems by Ram and Mottershead [4] and later extended to the multi-input multi-output case [5].

Classical feedback linearisation has found application in several areas. In the field of aeroelasticity, a series of papers [6–11] demonstrated theoretical and experimental application of the method to successfully control a pitch-plunge aeroelastic system. A recent publication by Jiffri et al. [12] followed a similar control approach, but with the inclusion of a real-time embedded tuned numerical model of the aeroelastic system in the control scheme. More recently, Castillo-Berrio and Feliu-Batlle [13] applied feedback linearisation experimentally to achieve precise beam-tip position control in a nonlinear two degrees of freedom flexible-beam sensor. A similar position control application was presented in [14], where Nanos and Papadopoulos applied feedback linearisation to ensure accurate path following of a space manipulator in the presence of joint flexibilities, which also had the effect of mitigating vibrations transmitted to the spacecraft supporting the manipulator. Choi and Ahn [15] experimentally implemented a feedback linearisation based controller for successful position and attitude control of a quadcopter. Alonge et al. [16] presented the theoretical development of a feedback linearisation based controller for the control of linear induction motor (LIM) drives with dynamic end effects which give rise to significant nonlinear behaviour. These results were later validated through experimental tests [17], which showed significant improvements when feedback linearisation was applied adaptively.

The application of classical input-output partial feedback linearisation was extended to systems with non-smooth nonlinearities by Jiffri et al. [18]. Experimental application of the method to the three degrees of freedom system discussed in this paper was successfully achieved by the present authors [19, 20], but significant effort was required to tune the numerical model to an adequate level of accuracy, in both the linear and nonlinear parameters, to successfully achieve the desired closed-loop dynamics. A special case was considered by Lisitano et al. [19] whereby control was applied to the same degree of freedom as the nonlinearity. In such a case, the system is linearised completely and the problem of determining the zero dynamics is trivialised to a check that the system is minimum phase. Lisitano et al. [20] considered the case when the nonlinearity was located at a different position, requiring a detailed and complex analysis to be carried out to establish the zero dynamics. The stability of the zero dynamics can alternatively be verified using the receptance method with a describing function (DF) approach [21], either using an analytical DF (as in the present case) or by carrying out a series of slow-sweep amplitude-controlled sine-excitation tests. An exposition of the theory of feedback linearisation by the receptance method was recently presented by Zhen et al. [22], and the purpose of the present paper is to demonstrate experimentally their findings, using the approach presented in that paper to replicate the closed-loop results already obtained for the three degrees of freedom test-rig with classical feedback linearisation by Lisitano et al. [20].

The subject of friction and impact in non-smooth nonlinear mechanical systems has long been studied by engineering scientists. For example, in 1995 Canudas de Wit et al. [23] combined the Dahl and Stribeck effects in a single model to represent both the effects of ‘stiction’ and decreasing friction with increasing velocity. They used the model to construct a friction observer and to carry out friction compensation in a tracking controller. More recently Giorgio and Scerrato [24] developed a multi-scale model, consisting of macro-, meso- and micro-scales, to represent rate-dependent internal friction in concrete. At the micro-scale, the model was of the Lu-Gre type that accounts for Coulomb friction and includes the Stribeck effect. Andreaus et al. [25] considered the dynamics of a cantilever beam that made contact with an obstacle in the form of a spring and viscous damper. Rather than an instantaneous impact, their model allowed for contact forces of finite duration governed by Heaviside functions, a single Heaviside function for the contact stiffness and double Heaviside functions for the contact damping. The resulting nonlinear differential equations were integrated numerically and validated by experiments. The same authors considered the microcantilever dynamics in tapping mode atomic force microscopy [26] including the van-der-Waals and Derjaguin–Muller–Toporov (DMT) contact forces.

In the present work, the form of the non-smooth nonlinearity is a piecewise stiffness (and damping) nonlinearity formed by the closure and opening of two gaps on either side of a linear spring. The stiffness is increased when the gap closes on one side and between the gaps the stiffness is linear. Friction is

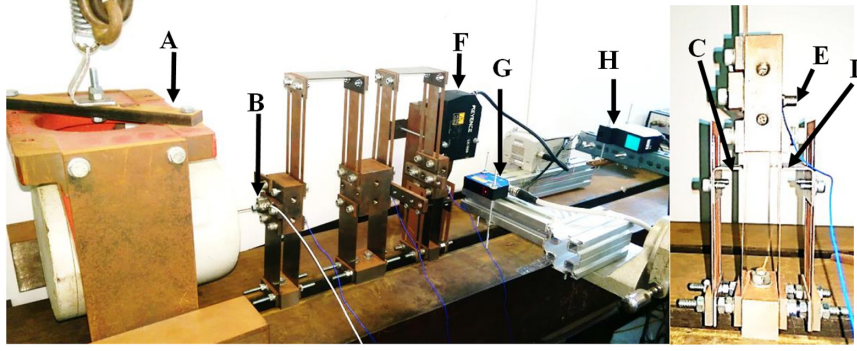


Figure 1. Non-smooth nonlinear system experimental setup. A: Suspended Shaker. B: Load cell. C: Left gap g_1 . D: Right gap g_2 . E: Accelerometers. F: Laser q_1 . G: Laser q_2 . H: Laser q_3 .

present during the periods that either gap is closed; its effect is represented by a Coulomb-type damping force proportional to the absolute stiffness force and directed in opposition to velocity. The effects of an instantaneous impact are neglected.

This paper is organised as follows. The experimental arrangement of the three degrees of freedom non-smooth nonlinear system is described in section 2 together with its actuation and sensors. In section 3, the system model, based on measured receptance data, and the complex DF with stiffness and damping terms is presented. Feedback linearisation theory is briefly described in section 4. In section 5 the results of preliminary tests are presented, showing inverse receptance terms, required by the theory, and the eigenvalues of the zero dynamics for different amplitudes of sinusoidal displacement. Finally, in section 6, the results of experimental implementation of the receptance-based feedback linearisation method are presented, both in the frequency and time domains.

2. Experimental arrangement

The experimental system shown in Figure 1 consists of three masses, degrees of freedom 1, 2 and 3 from left to right, supported and connected by thin plate-like springs. The system includes a non-smooth structural nonlinearity in the form of a piecewise-linear spring arrangement located at the third degree of freedom. This is achieved by adding two springs, known as setting springs, mounted on either side of the third mass with continuously adjustable separation (gaps g_1 left and g_2 right) from the grounding (or support) springs. This arrangement produces the non-smooth nonlinear hardening stiffness characteristic shown in Figure 2, depending upon the gaps being open or closed. The nonlinear effect can be modified by changing the extent of the gaps and/or the lengths l of the setting spring (i.e. the vertical contact location). The settings chosen for the experiments carried out in this paper were $g_1 = g_2 = 0.035$ mm and $l = 81.6$ mm.

Excitation could be applied either by an instrumented hammer (PCB 086C03) or the suspended shaker (LDS V406) with the LDS PA100 amplifier. Load cell PCB 208C02 was used to measure the force applied by the shaker with PCB 442C04 ICP signal conditioner. Laser displacement measurements (Keyence LK-500 and LK-G402, and microepsilon OptoNCDT 1402-100) were available and acceleration sensors (K-Shear 8728A500) were mounted on each of the three masses with PCB 442C04 ICP signal conditioners. Displacements and velocities were used in control experiments with velocities determined by numerical differentiation of laser displacement measurements.

Hammer excitation and accelerometers were used with a Siemens LMS Test.Lab system for the determination of receptances for the underlying linear system (i.e. with the setting springs removed) and for the partially linearised closed-loop system. The closed-loop control force was applied using the shaker, and implemented using dSPACE (10 kHz sampling speed) within a nested controller, as shown in Figure 3. The inner PD loop is present to ensure that the desired control force has indeed been applied, this being necessary because the shaker is current controlled and therefore its force is not proportional to the dSPACE command voltage. A Butterworth filter with a cut-off frequency of 21 Hz was used to

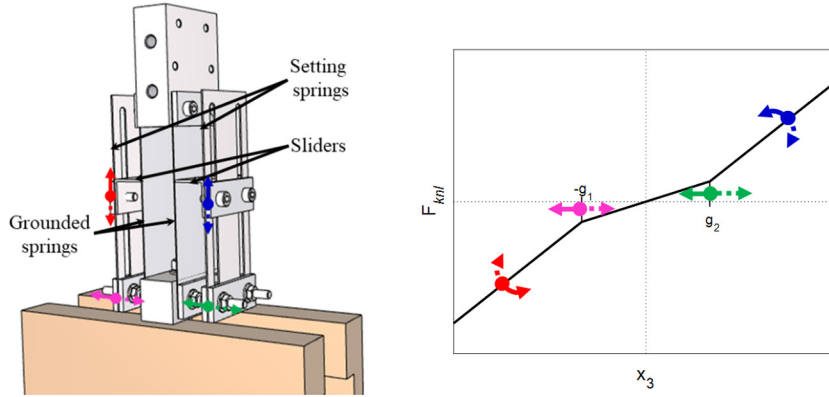


Figure 2. Nonlinear spring model (left), nonlinear spring characteristic (right).

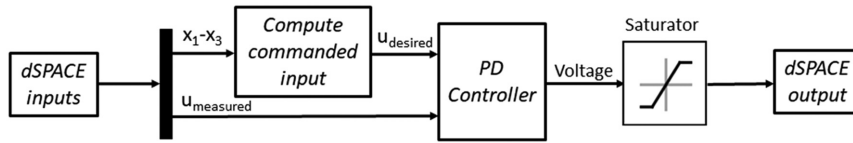


Figure 3. Nested controller.

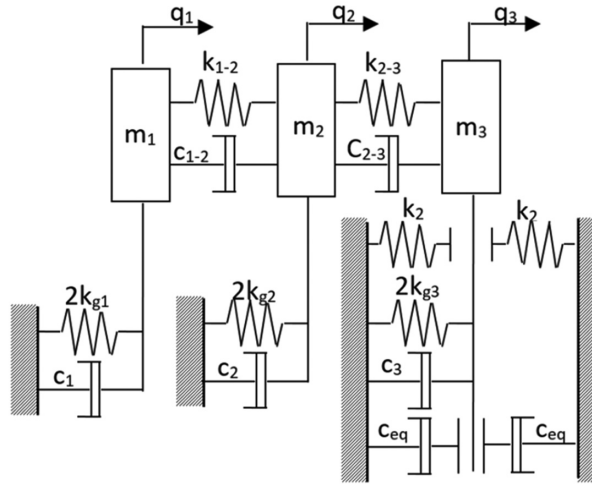


Figure 4. Schematic of the three degrees of freedom non-smooth nonlinear system.

remove high frequency noise and the saturator shown in the figure was present to prevent damage that might otherwise be caused to the shaker should the armature hit the end stops.

3. Receptance-based model

The system may be represented as shown in Figure 4, as a three degrees of freedom arrangement of lumped masses connected by springs and light dampers. It is seen that one of the two springs labelled k_2 becomes active when the motion of mass m_3 is great enough to close the gap. The dampers c_{eq} represent Coulomb friction when the gap, $g = \begin{cases} g_1 \\ g_2 \end{cases}$, is closed.

One advantage of the receptance method is that a mathematical model of the usual \mathbf{M} , \mathbf{C} , \mathbf{K} (mass, damping, stiffness) form is unnecessary and instead the system is represented by experimentally acquired receptance measurements. Thus, the underlying linear system, for small displacements such that the gaps remain open, is given by

$$\mathbf{H}(i\omega)\mathbf{f}(t) = \mathbf{x}(t) \quad (1)$$

and, in the Laplace 's' domain by modal synthesis

$$\mathbf{H}(s) = \sum_{j=1}^3 \frac{\boldsymbol{\psi}_j \boldsymbol{\psi}_j^T}{a_j(s - \lambda_j)} + \frac{\boldsymbol{\psi}_j^* \boldsymbol{\psi}_j^{*T}}{a_j^*(s - \lambda_j^*)}; \quad s = i\omega \quad (2)$$

where $\boldsymbol{\psi}_j$ is the j^{th} eigenvector, λ_j is the j^{th} pole and a_j is a modal constant. $(\bullet)^*$ denotes complex conjugation. In theory, assuming the \mathbf{M} , \mathbf{C} , \mathbf{K} matrices to be known, the receptance transfer function matrix may be expressed as $\mathbf{H}(s) = (\mathbf{M}s^2 + \mathbf{C}s + \mathbf{K})^{-1}$.

If the displacement of m_3 is such that the gap becomes closed, then the system behaviour is nonlinear and an amplitude-dependent linearised receptance model may be obtained by swept sine testing

$$\mathbf{H}_{nl}(X, i\omega)\mathbf{f}(t) = \mathbf{x}(t) \quad (3)$$

where

$$x_3 = X \sin \omega t; \quad \omega = \Omega t \quad (4)$$

and the sweep rate, Ω , is very low in comparison to the natural frequencies of the system.

Equations (3) and (4) are the equivalent of the DF representation of stiffness k_2 and damper c_{eq} acting on m_3 . Gelb and Vander Velde [21] give the DF of the stiffness term as

$$N_{Knl}(X) = k_2[1 - \alpha(\chi)] \quad (5)$$

where

$$\alpha(\chi) = \begin{cases} -1 & \chi < -1 \\ \frac{2}{\pi} \left(\sin^{-1}(\chi) + \chi \sqrt{1 - \chi^2} \right) & |\chi| \leq 1 \\ 1 & \chi > 1 \end{cases}, \quad \chi = \frac{g}{X} \quad (6)$$

The nonlinear damper force was represented using a Coulomb model by the present authors as

$$f_{Cnl,3} = \varepsilon |f_{Knl,3}| \text{sign}(\dot{x}_3) \quad (7)$$

where

$$f_{Knl,3} = \begin{cases} k_2(x_3 - (-g)) & q_3 \leq -g \\ 0 & -g \leq x_3 \leq g \\ k_2(x_3 - g) & q_3 \geq g \end{cases} \quad (8)$$

The DF for the nonlinear damper is developed in the Appendix and given here as

$$N_{Cnl}(X) = -i \frac{2\varepsilon k_2}{\pi} (1 - \beta(\chi))^2 \quad (9)$$

where

$$\beta(\chi) = \begin{cases} -1 & \chi < -1 \\ \chi & |\chi| \leq 1 \\ 1 & \chi > 1 \end{cases}, \quad \chi = \frac{g}{X} \quad (10)$$

Thus, the total DF, including stiffness and damping is

$$N_{nl}(X) = N_{Knl}(X) + N_{Cnl}(X) = k_2 \left([1 - \alpha(\chi)] - i \frac{2\varepsilon}{\pi} (1 - \beta(\chi))^2 \right) \quad (11)$$

or, when written in the Laplace ‘s’ domain,

$$N_{nl}(X, s) = k_2 \left([1 - \alpha(\chi)] - s \frac{2\varepsilon}{\pi\omega} (1 - \beta(\chi))^2 \right) \quad (12)$$

If the linear receptance matrix, equation (1) is available and the DF known, then the amplitude-dependent receptance, equation (3), may be computed by using the Sherman–Morrison formula [27, 28]

$$\mathbf{H}_{nl}(X, s) = \mathbf{H}(s) - \frac{N_{nl}(X, s) \mathbf{H}(s) \mathbf{e}_i \mathbf{e}_i^T \mathbf{H}(s)}{1 + N_{nl}(X, s) \mathbf{e}_i^T \mathbf{H}(s) \mathbf{e}_i} \quad (13)$$

where \mathbf{e}_i is the unit vector given by the i^{th} column of the identity matrix and i denotes the location of the nonlinearity. If the DF is unknown, then it may be determined by inverse DF methods, typically [29, 30].

4. Feedback linearisation by the method of receptances

The theory of feedback linearisation by the receptance method is given in detail by Zhen et al. [22]. A summary is provided here for purposes of completeness. To begin, equation (1) may be re-written in the form

$$\mathbf{x}(s) = \mathbf{H}_{nl}(X, s) \mathbf{B} \mathbf{u}(s) \quad (14)$$

where \mathbf{B} is the force distribution matrix and

$$\mathbf{x} = \begin{pmatrix} \mathbf{x}_1 \\ \mathbf{x}_2 \end{pmatrix}; \quad \dim(\mathbf{x}_1) = \dim(\mathbf{u}(s)) \quad (15)$$

and the output is given by

$$\mathbf{y}(s) = \mathbf{x}_1(s) \quad (16)$$

A coordinate transformation is then defined with the purpose of separating the system into two parts, controllable and uncontrollable, known as the normal form. Thus

$$\mathbf{z} = \mathbf{T} \mathbf{x}; \quad \mathbf{T} = \begin{bmatrix} \mathbf{I} & \mathbf{0} \\ \mathbf{0} & \mathbf{V} \end{bmatrix} \quad (17)$$

where

$$\mathbf{V} \mathbf{B} = \mathbf{0}; \quad \mathbf{V} \mathbf{V}^T = \mathbf{I} \quad (18)$$

In the case of the three degrees of freedom system shown in Figure 4, the terms in equations (17) and (18) are given by, $\mathbf{B} \in \mathbb{R}^{3 \times 1}$, $\mathbf{V} \in \mathbb{R}^{2 \times 3}$, $\mathbf{0} = [0 \ 0]$ and \mathbf{I} denotes the identity matrix of appropriate dimension.

Then, in transformed coordinates and using partitioning consistent with that in equations (15) and (17),

$$\begin{bmatrix} \mathbf{z}_1(s) \\ \mathbf{z}_2(s) \end{bmatrix} = \begin{bmatrix} (\tilde{\mathbf{H}}_{nl}(Z, s))_{11} & (\tilde{\mathbf{H}}_{nl}(Z, s))_{12} \\ (\tilde{\mathbf{H}}_{nl}(Z, s))_{21} & (\tilde{\mathbf{H}}_{nl}(Z, s))_{22} \end{bmatrix} \begin{bmatrix} \mathbf{B}_1 \mathbf{u}(s) \\ \mathbf{0} \end{bmatrix} \quad (19)$$

where

$$\tilde{\mathbf{H}}_{nl} = \mathbf{T}^T \mathbf{H}_{nl} \mathbf{T} \quad (20)$$

Inverting equation (19) leads to

$$\begin{bmatrix} \mathbf{B}_1 \mathbf{u}(s) \\ \mathbf{0} \end{bmatrix} = \begin{bmatrix} \left((\tilde{\mathbf{H}}_{nl}(Z, s))^{-1} \right)_{11} & \left((\tilde{\mathbf{H}}_{nl}(Z, s))^{-1} \right)_{12} \\ \left((\tilde{\mathbf{H}}_{nl}(Z, s))^{-1} \right)_{21} & \left((\tilde{\mathbf{H}}_{nl}(Z, s))^{-1} \right)_{22} \end{bmatrix} \begin{bmatrix} \mathbf{z}_1(s) \\ \mathbf{z}_2(s) \end{bmatrix} \quad (21)$$

and, if the control input is chosen, as

$$\mathbf{u}(s) = \mathbf{B}_1^{-1} \left[\tilde{\mathbf{u}}(s) + \left((\tilde{\mathbf{H}}_{nl}(Z, s))^{-1} \right)_{11} \mathbf{z}_1(s) + \left((\tilde{\mathbf{H}}_{nl}(Z, s))^{-1} \right)_{12} \mathbf{z}_2(s) - \text{diag}(s^2) \mathbf{z}_1(s) \right] \quad (22)$$

then the first row of equation (21) is linearised and may be written as

$$\text{diag}(s^2) \mathbf{z}_1(s) = \tilde{\mathbf{u}}(s) \quad (23)$$

where $\tilde{\mathbf{u}}(s)$ is an artificial input. It should be noted that equation (22) must be implemented in the time domain, which requires the form of the nonlinearity to be known, either explicitly (as in the present case) or by inversion of a DF.

A pole μ_k may be assigned when

$$\tilde{\mathbf{u}}(s) = -(\mu_k \mathbf{F}^T + \mathbf{G}^T) \mathbf{z}_1(\mu_k) \quad (24)$$

and control gains $\mathbf{F} = \text{diag}(\bar{f}_k)$ and $\mathbf{G} = \text{diag}(\bar{g}_k)$ are given by

$$\begin{aligned} \bar{f}_k &= -(\mu_k + \mu_k^*) \\ \bar{g}_k &= \mathbb{R}(\mu_k \mu_k^*) \end{aligned} \quad (25)$$

For the system to be stable, not only must the poles of the controllable part be stable, but also the so-called zero dynamics must be stable. The zero dynamics are those of the uncontrollable system (known as the internal dynamics) when the controlled degrees of freedom are set to zero. Zhen et al. [22] showed that the zero dynamics were stable if, and only if, the poles of the transfer function

$$(\tilde{\mathbf{H}}_{nl}(Z, s))_{22} - (\tilde{\mathbf{H}}_{nl}(Z, s))_{21} (\tilde{\mathbf{H}}_{nl}(Z, s))_{11}^{-1} (\tilde{\mathbf{H}}_{nl}(Z, s))_{12} \quad (26)$$

are stable for the range of all amplitudes Z of vibrations of the system. The measured receptance matrix of the linear system may be combined with the DF approximation of the system nonlinearities to compute the amplitude-dependent nonlinear receptance matrix, as in equations (20) and (13), from which the expression (26) may be found.

5. Preliminary tests

Experimental and synthesised frequency response functions (using equation (2)) of the underlying linear system are presented in Figure 5, where very close agreement can be observed.

Elements of the inverse receptance matrix (i.e. the experimental dynamic stiffness matrix) are required in equations (22) and (26) and shown in Figure 6, where inversion of both the measured and synthesised FRFs are shown to be in almost perfect agreement.

The nonlinear receptances obtained from equation (13) for different values of X are shown in Figure 7. In the experimental example considered here, there is a single (scalar) control input $u(s)$

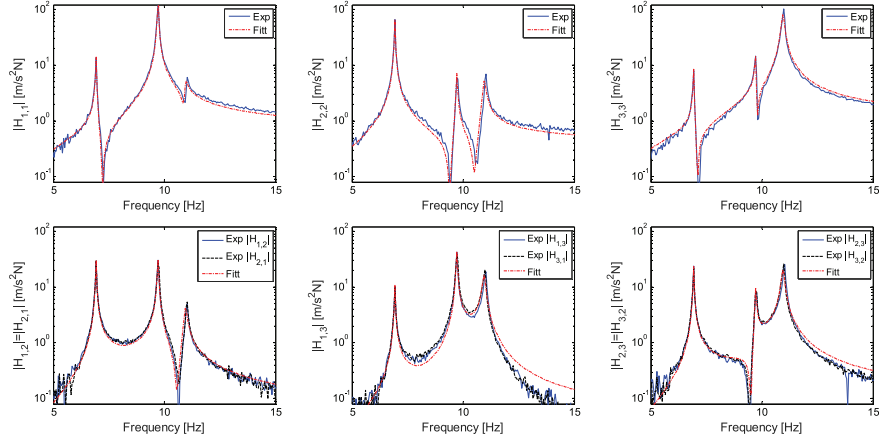


Figure 5. Experimental and synthesised FRFs.

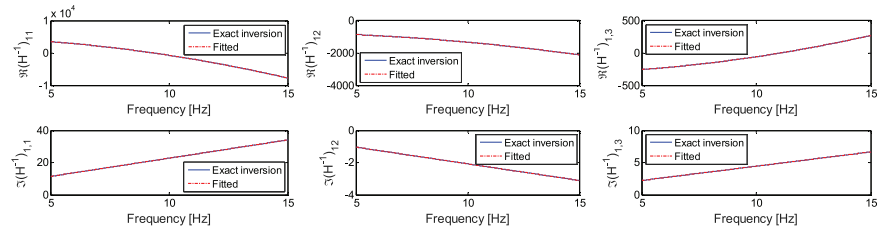


Figure 6. Inverse receptance terms (dynamic stiffness).

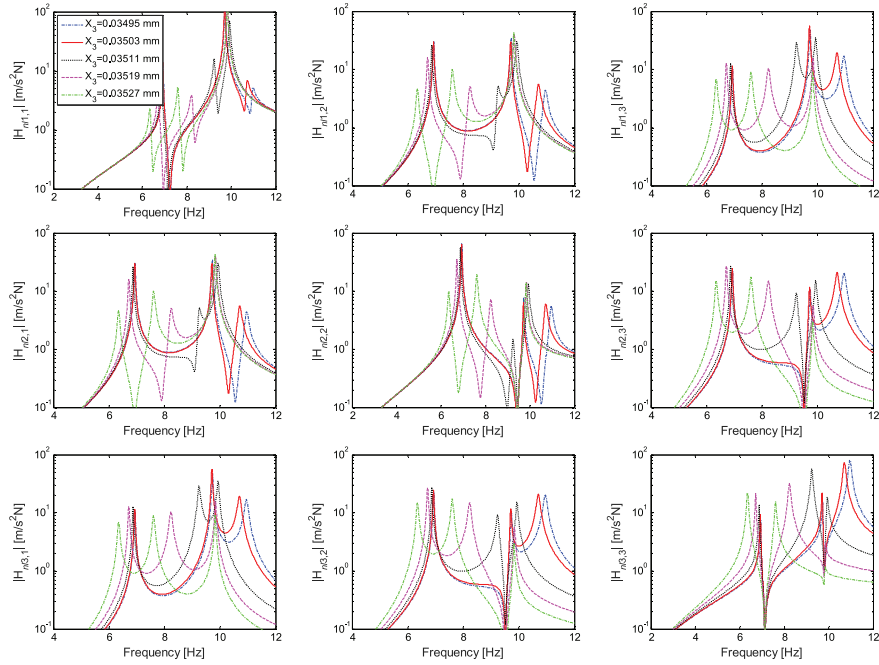


Figure 7. FRF matrix of the nonlinear system, changing amplitude.

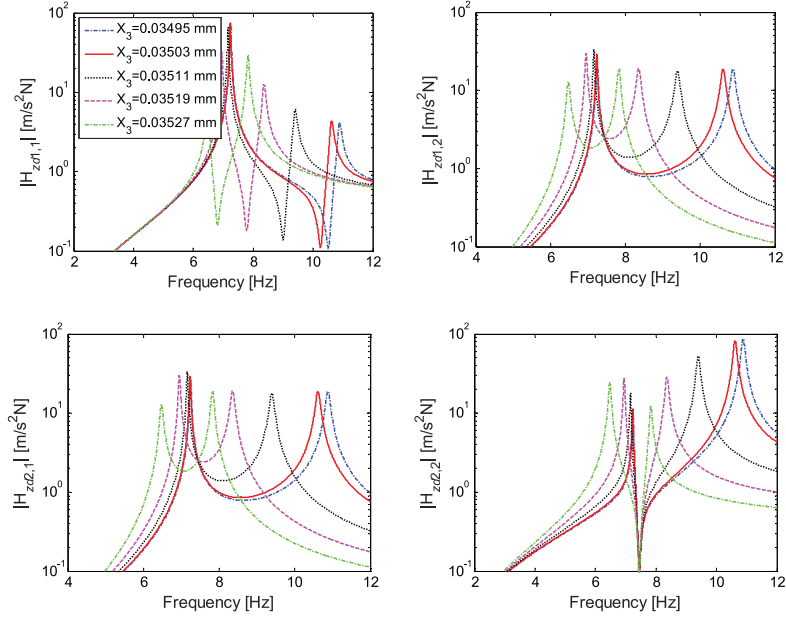


Figure 8. Zero dynamics FRF changing \mathbf{X} amplitude.

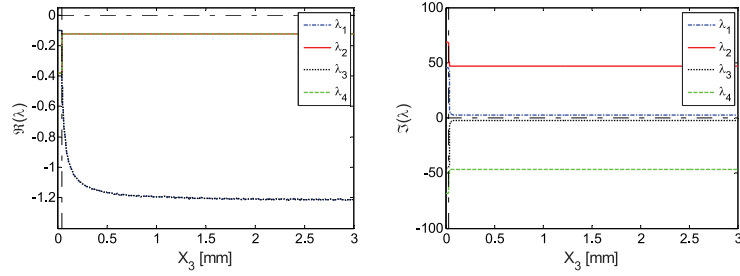


Figure 9. Poles of the zero dynamics: real part (left), imaginary part (right).

applied at the first degree of freedom. Therefore, \mathbf{B} in equation (14) is a 1×3 vector, $\mathbf{b} = (1 \ 0 \ 0)^T$ and the transformation matrix in equation (17) may be written as the identity matrix, $\mathbf{T} = \mathbf{I}_{3 \times 3}$ so that the two systems of coordinates referred to earlier are identical, that is $\mathbf{z} = \mathbf{x}$. Parameters ε and k_2 are chosen to take values of 0.3954 and 1722.6 N/m, having been identified previously as reported by the present authors [20].

The transfer function matrix of the zero dynamics determined by using the amplitude-dependent receptances in equation (26) are shown in Figure 8. The loci of the zero dynamics poles, extracted by using rational fractional polynomials, are shown in Figure 9, and Figure 10 shows an enlarged view close to the gap at $X = 0.035$ mm.

Having established that the zero dynamics are stable, pole placement may be carried out as described in the following section.

6. Results from the closed-loop system

In this section, experimental results produced by the receptance-based partial feedback linearisation approach described in section 4 are presented and compared to numerically-produced results from a \mathbf{M} , \mathbf{C} , \mathbf{K} model described in the authors' previous research [20] and shown schematically in Figure 3. Inspection of equations (14) and (19) [20] shows that the dynamics of the controlled degrees of freedom are independent of the internal dynamics, but the dynamics of uncontrolled degrees of freedom (the

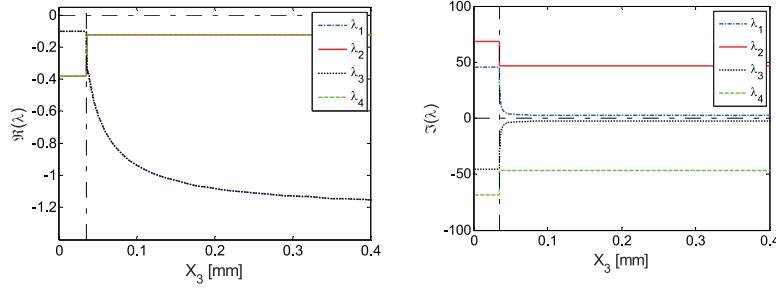


Figure 10. Zoomed view of poles: real part (left), imaginary part (right).

internal dynamics) depend upon all the degrees of freedom of the system. Then, since $\mathbf{T} = \mathbf{I}_3 \times 3$ and $\mathbf{z} = \mathbf{x}$, it is clear that the first degree of freedom is linearised and the closed-loop receptance $\mathbf{H}_{11}^{cl}(s)$ has only a single degree of freedom and a single natural frequency. Thus, with the controller switched on, an impact hammer test at the first degree of freedom is sufficient to fully characterise the dynamics of the linearised part of the closed-loop system. In the present example, the controller was used to assign the natural frequency $\omega_n = 2\pi f_n$ and damping ratio ζ_n of the first degree of freedom. Displacements were recorded for 10 s from the moment of impact, and experimental FRFs obtained by averaging over five tests.

Experiments and numerical simulations were repeated for three different values of assigned natural frequencies, $\omega_n = 2\pi f_n = \{13.5 \ 16 \ 19\}$ Hz, and 12 damping ratios, $\zeta_n = \{0.5 \ 1 \ 5 \ 10 \ 15 \ 20 \ 25 \ 30 \ 35 \ 40 \ 45 \ 50\}\%$. Not all the damping values were achievable because, for higher values of natural frequencies and very low values of damping ratios, the shaker saturated and was not able to deliver the required input force to the system. The amplitude of vibration was sufficient to induce nonlinearity by gap closure in all the tests, until the motion decayed sufficiently for the gaps to remain open. The experimental closed-loop FRFs of the linearised degree of freedom are shown in Figure 11. It is seen that the controller was able to assign the desired dynamics in almost all cases. The open-loop dynamics of the system were completely cancelled out, thus confirming the accuracy of the extracted open-loop receptances. It was observed that when the assigned values of natural frequency were low, a small portion of the dynamics of the first mode was not completely cancelled out, most likely due to imperfect synthesis of measured FRFs. Experimental results appear to be in very good agreement with their numerical counterparts shown in Figure 12. Successful linearisation is evident also from the expected presence of just a single peak in the closed-loop response. The response of the linearised system at low frequencies is higher in the experiments than in numerical simulation, most likely due to motion of the shaker in the low frequency range.

The natural frequencies and damping ratios of the closed-loop system are compared to assigned values in Figure 13. The poles are correctly identified until $\zeta_n = 30\text{--}35\%$ in the closed-loop FRFs. For very high levels of damping ratio, the identification is no longer feasible, although from the experimental FRFs it is clear that the damping is increasing. Successful assignment of the desired natural frequency through feedback linearisation is possible in almost all the cases in which a pole is identified. When the assigned natural frequency is $f_n = 13.5$ Hz (red bars in the online version of Figure 13) the actual natural frequency is very close to the assigned value in all performed tests. The damping ratio is assigned accurately until 25%, beyond which value there is a growing discrepancy between assigned and actual value; there is, however, a trend of increasing damping. In the case of $f_n = 16$ Hz (black bars in the online version of Figure 13), the minimum achievable damping ratio is $\zeta_n = 3.5\%$, because the shaker saturates for lower values. The experimental natural frequencies are all well aligned with assigned values in the cases in which tests can be performed, while the damping ratios are slightly less than the desired values. In the last case, $f_n = 19$ Hz (green bars in the online version of Figure 13), the effect of actuator saturation is clearly visible – the minimum damping ratio assignable is $\zeta_n = 7.5\%$. It is seen that in this case also the controller continues to assign natural frequencies very well, while the damping ratios in this case also follow the increasing trend but are not close to the assigned values.

Analysing the phases of the linearised degree of freedom, the assigned natural frequencies are located very close to the -90° phase point, as in Figure 14. The slope of the phase decreases with increasing damping ratio, thereby confirming the expected increased damping.

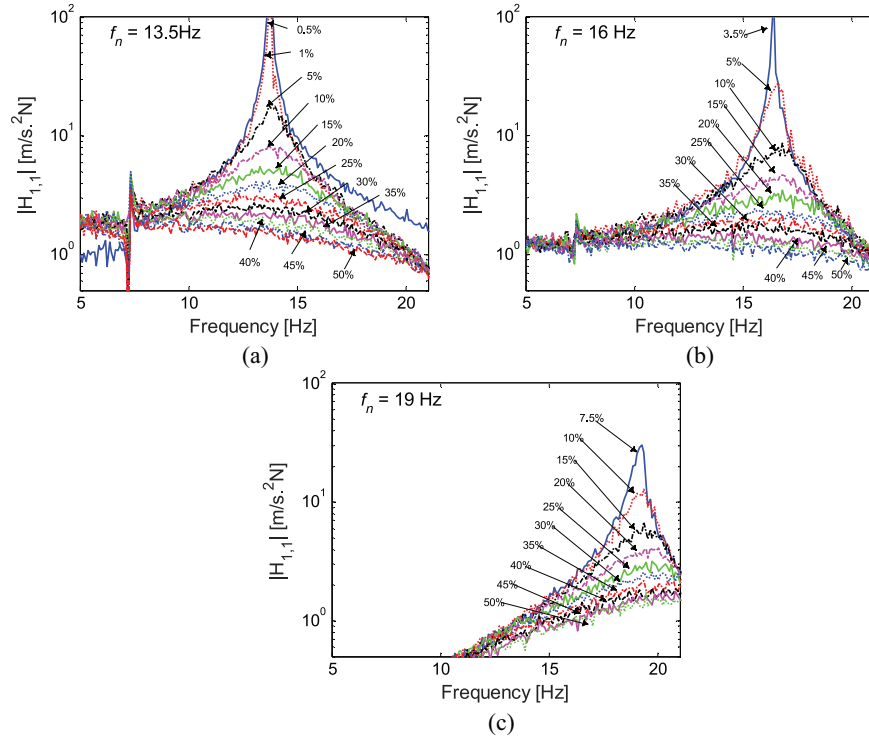


Figure 11. Experimental closed-loop FRFs.

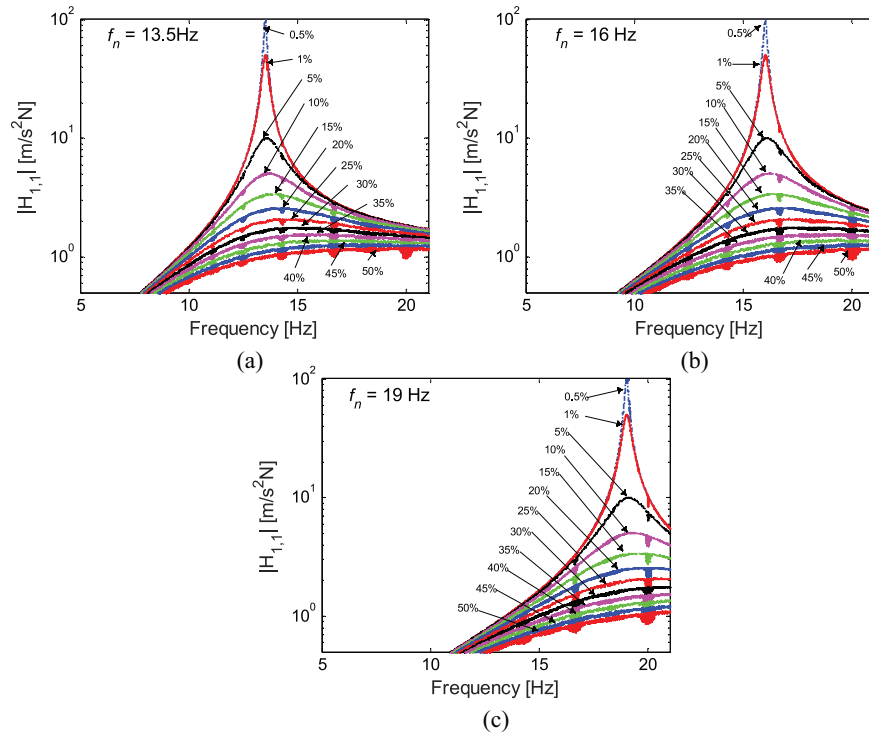


Figure 12. Numerical closed-loop FRFs.

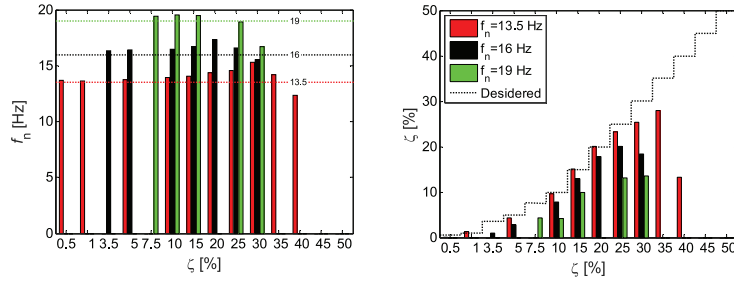


Figure 13. Feedback linearisation $f_n = 13.5, 16$ and 19 Hz.

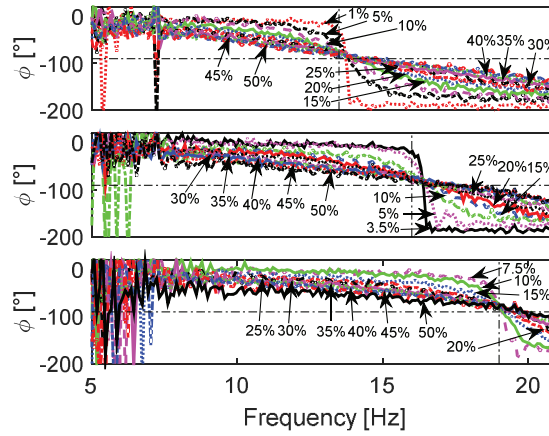


Figure 14. Experimental closed-loop FRF phases.

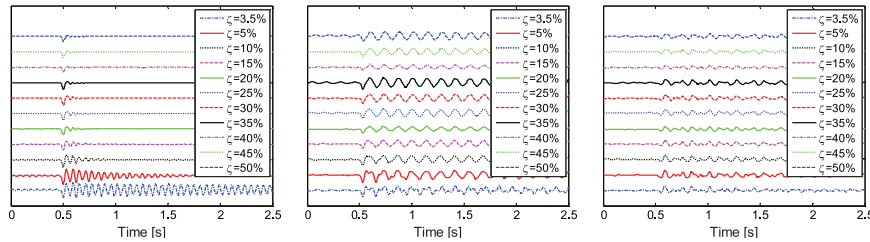


Figure 15. Time domain responses for $f_n = 16$ Hz (left z_1 , middle z_2 , right z_3).

The experimental time domain responses of the controlled (z_1), and uncontrolled degrees of freedom (z_2, z_3), reflect the observations seen in the above frequency domain plots. Results for the case of $f_n = 16$ Hz are shown in Figure 15. A single harmonic, very close to the assigned frequency is visible in the z_1 response (Figure 15 left). The decay time of the response clearly decreases when the damping ratio is increased, which reflects successful assignment of the damping.

Although the first degree of freedom is linearised by the controller, the internal dynamics (second and third degrees of freedom) remains nonlinear. The FRFs pertaining to the third degree of freedom for the various values of natural frequencies and damping ratios assigned to the first (controlled) degree of freedom are shown in Figures 16 and 17 for the numerical and experimental cases, respectively. The expected multi-mode dynamic behaviour is evident from these plots; there are two fixed resonances at

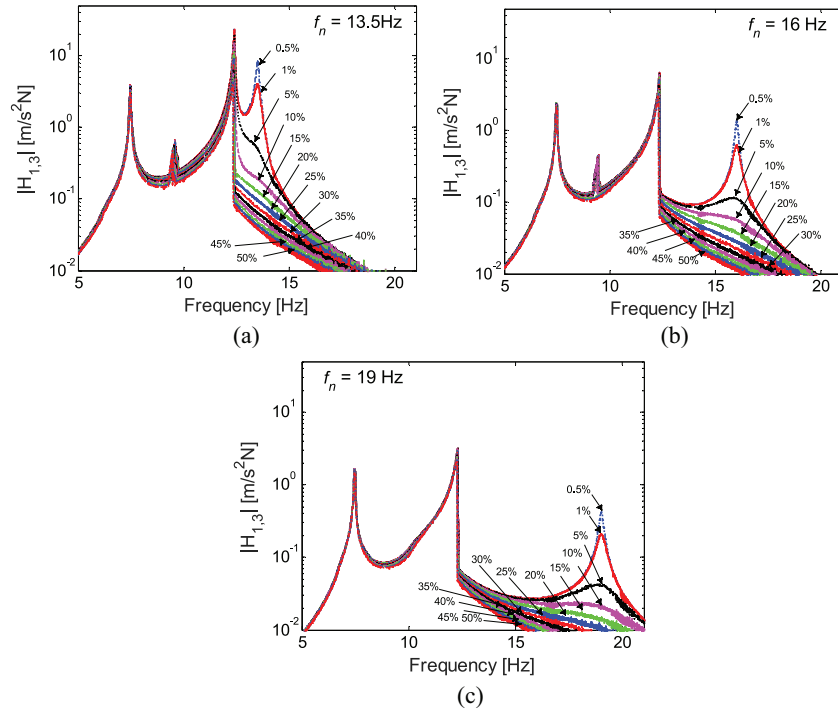


Figure 16. Numerical closed-loop internal dynamics $H_{1,3}$.

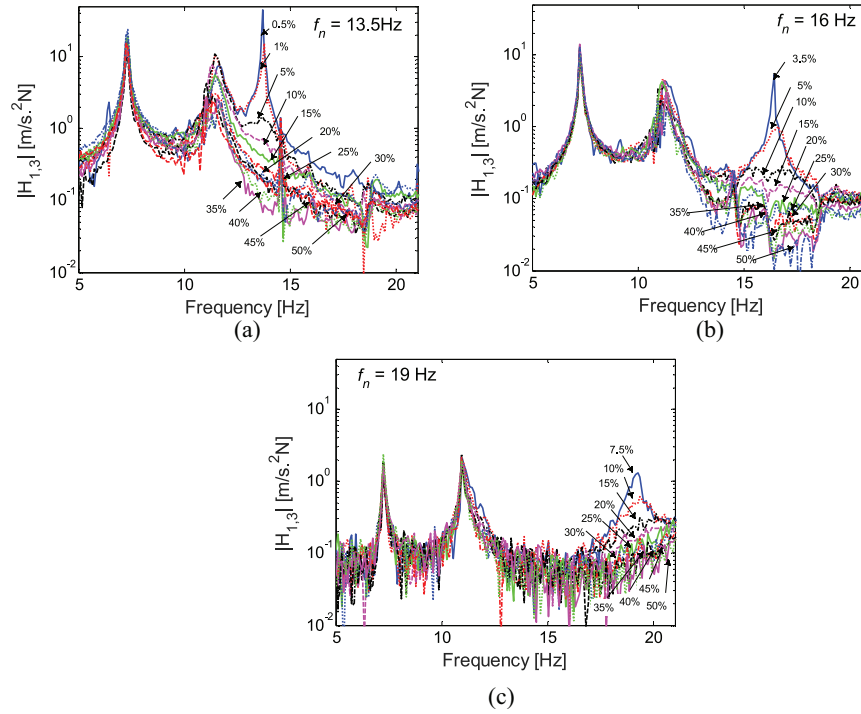


Figure 17. Experimental closed-loop internal dynamics $H_{1,3}$.

natural frequencies corresponding to the first and third open-loop modes, and a third peak corresponding to the dynamics assigned to the first degree of freedom. The clearly visible jump in the numerical simulations of $H_{1,3}$ is not visible in the experimental results because the FRFs were obtained from hammer tests.

The z_2, z_3 time domain plots of the internal dynamics (Figure 15 middle and right) with smaller amplitude-scale than z_1 , exhibit multi-harmonic behaviour. Although the decay time for z_2, z_3 is clearly much longer than that of z_1 , the system was found to be completely at rest after 15 s.

7. Conclusion

The application of a new control approach that combines partial feedback linearisation with the receptance method, previously studied theoretically and in simulation, is experimentally investigated in this paper. The new method is able to linearise the system without the necessity of a system model, thereby eliminating errors due to inaccuracies in the numerical representation of the system. The controller is implemented on a three degree of freedom nonlinear system with a piecewise-linear stiffness characteristic. With the input and output at the first degree of freedom, the nonlinearity is located at the third degree of freedom. The control configuration results in the internal dynamics being non-smooth, and its stability is studied using a receptance-based method. Partial feedback linearisation is successfully achieved, with the linearised (first) degree of freedom displaying a single mode at the assigned natural frequency while the other modes are almost completely cancelled out, except for small discrepancies when the assigned natural frequency is low. The agreement between desired and actual values of natural frequencies and damping ratios is very good, except for a few cases when a pole cannot be identified or the shaker saturates.


Acknowledgements

The research described in this paper was carried out during a visit to the University of Liverpool by the first author, Domenico Lisitano.

Funding

Domenico Lisitano wishes to acknowledge support provided by an Erasmus+Traineeship funded by the European Commission.

ORCID iD

Domenico Lisitano  <https://orcid.org/0000-0003-4882-4554>

References

- [1] Isidori, A. *Nonlinear control systems*. Berlin, Heidelberg, New York: Springer, 1995.
- [2] Khalil, HK. *Nonlinear systems*: Prentice Hall, New Jersey, 2002.
- [3] Vidyasagar, M. *Nonlinear systems analysis* (2nd edn). New Jersey: Prentice-Hall, Inc., 1992.
- [4] Ram, YM, and Mottershead, JE. Receptance method in active vibration control. *AIJA J* 2007; 45, 3: 562–567.
- [5] Ram, YM, and Mottershead, JE. Multiple-input active vibration control by partial pole placement using the method of receptances. *Mech Syst Sig Process* 2013; 40, 2: 727–735. doi: <http://dx.doi.org/10.1016/j.ymssp.2013.06.008>
- [6] Ko, J, Kurdila, AJ, and Strganac, TW. Nonlinear control of a prototypical wing section with torsional nonlinearity. *J Guid Contr Dynam* 1997; 20, 6: 1181–1189. doi: 10.2514/2.4174
- [7] Ko, J, Kurdila, AJ, and Strganac, T. Stability and control of a structurally nonlinear aeroelastic system. *J Guid Contr Dynam* 1998; 21: 718–725.
- [8] Block, JJ, and Strganac, TW. Applied active control for a nonlinear aeroelastic structure. *J Guid Contr Dynam* 1998; 21, 6: 838–845. doi: 10.2514/2.4346
- [9] Ko, J, Strganac, TW, and Kurdila, AJ. Adaptive feedback linearization for the control of a typical wing section with structural nonlinearity. *Nonlin Dynam* 1999; 18, 3: 289–301. doi: 10.1023/a:1008323629064
- [10] Strganac, T, Ko, J, and Thompson, D. Identification and control of limit cycle oscillations in aeroelastic systems. *J Guid Contr Dynam* 2000; 23, 6: 1127–1133.

- [11] Platanitis, G, and Strganac, TW. Control of a nonlinear wing section using leading- and trailing-edge surfaces. *J Guid Contr Dynam* 2004; 27, 1: 52–58. doi: 10.2514/1.9284
- [12] Jiffri, S, Fichera, S, Mottershead, JE, and Da Ronch, A. Experimental nonlinear control for flutter suppression in a nonlinear aeroelastic system. *J Guid Contr Dynam* 2017; 40, 8: 1925–1938. doi: 10.2514/1.G002519
- [13] Castillo-Berrio, CF, and Feliu-Batlle, V. Vibration-free position control for a two degrees of freedom flexible-beam sensor. *Mechatronics* 2015; 27: 1–12. doi: <http://dx.doi.org/10.1016/j.mechatronics.2015.01.005>
- [14] Nanos, K, and Papadopoulos, EG. On the dynamics and control of flexible joint space manipulators. *Contr Eng Pract* 2015; 45: 230–243. doi: <http://dx.doi.org/10.1016/j.conengprac.2015.06.009>
- [15] Choi, YC, and Ahn, HS. Nonlinear control of quadrotor for point tracking: Actual implementation and experimental tests. *IEEE/ASME Trans Mechatronics* 2015; 20, 3: 1179–1192. doi: 10.1109/TMECH.2014.2329945
- [16] Alonge, F, Cirrincione, M, Pucci, M, and Sferlazza, A. Input–output feedback linearizing control of linear induction motor taking into consideration the end-effects. Part I: Theoretical analysis. *Contr Eng Pract* 2015; 36: 133–141. doi: <http://dx.doi.org/10.1016/j.conengprac.2014.08.009>
- [17] Alonge, F, Cirrincione, M, Pucci, M, and Sferlazza, A. Input–output feedback linearizing control of linear induction motor taking into consideration the end-effects. Part II: Simulation and experimental results. *Contr Eng Pract* 2015; 36: 142–150. doi: <http://dx.doi.org/10.1016/j.conengprac.2014.09.013>
- [18] Jiffri, S, Paoletti, P, and Mottershead, JE. Feedback linearization in systems with non-smooth nonlinearities. *J Guide Contr Dynam* 2016; 39, 4: 814–825. doi: 10.2514/1.g001220
- [19] Lisitano, D, Zhen, C, and Jiffri, S, Bonisoli, E, and Mottershead J.E. An example of feedback linearization in a non-smooth system. In: *International Conference on Structural Engineering Dynamics* Ericeira, Portugal, 3–5 July 2017, Universidade de Lisboa, Instituto Superior Técnico paper no. 030.
- [20] Lisitano, D, Jiffri, S, and Bonisoli, E, and Mottershead, J.E. Experimental feedback linearisation of a vibrating system with a non-smooth nonlinearity. *J Sound Vibration* (in press).
- [21] Gelb, A, and Vander Velde, WE. *Multiple-input describing functions and nonlinear system design*. New York: McGraw-Hill, 1968.
- [22] Zhen, C, Jiffri, S, and Li, D, Li, D. and Mottershead, J.E. Feedback linearisation of nonlinear vibration problems: A new formulation by the method of receptances. *Mech Syst Sig Process* 2018; 98:1056–1068. doi: <http://dx.doi.org/10.1016/j.ymssp.2017.05.048>
- [23] de Wit, CC, Olsson, H, and Astrom, KJ, and Lischinsky, P. A new model for control of systems with friction. *IEEE Trans Auto Contr* 1995; 40, 3: 419–425. doi: 10.1109/9.376053
- [24] Giorgio, I, and Scerrato, D. Multi-scale concrete model with rate-dependent internal friction. *Euro J Environ Civil Eng* 2016; 21, 7–8: 821–839. doi: <http://dx.doi.org/10.1080/19648189.2016.1144539>
- [25] Andreus, U, Baragatti, P, and Placidi, L. Experimental and numerical investigations of the responses of a cantilever beam possibly contacting a deformable and dissipative obstacle under harmonic excitation. *Int J Non-Lin Dynam* 2016; 80: 96–106. doi: <https://doi.org/10.1016/j.ijnonlinmec.2015.10.007>
- [26] Andreus, U, Placidi, L, and Rega, G. Microcantilever dynamics in tapping mode atomic force microscopy via higher eigenmodes analysis. *J Appl Phys* 2013; 113: 224302. doi: <http://dx.doi.org/10.1063/1.4808446>
- [27] Golub, GH, and Loan, CFV. *Matrix computations*. Baltimore, MD: Johns Hopkins University Press, 1983, 51.
- [28] Mottershead, JE, and Ram, YM. Inverse eigenvalue problems in vibration absorption: Passive modification and active control. *Mech Syst Sig Process* 2006; 20, 1: 5–44. doi: <http://dx.doi.org/10.1016/j.ymssp.2005.05.006>
- [29] Nassirharand, A, and Karimi, H. Nonlinear controller synthesis based on inverse describing function technique in the MATLAB environment. *Adv Eng Softw* 2006; 37, 6: 370–374. doi: <http://dx.doi.org/10.1016/j.advengsoft.2005.09.009>
- [30] Nassirharand, A. Matlab software for inversion of describing functions. *Adv Eng Softw* 2009; 40, 8: 600–606. doi: <http://dx.doi.org/10.1016/j.advengsoft.2008.11.003>

Appendix

The nonlinear damping force, as given in equation 7, is represented in the F - x plane as shown in Figure 18. The DF is defined as

$$N_{Cnl}(\omega, a) = n_p + in_q = n_p + \frac{n_q}{\omega} s \quad (27)$$

Because in this case the force is a dissipative force, the cycle is in the counter-clockwise direction.

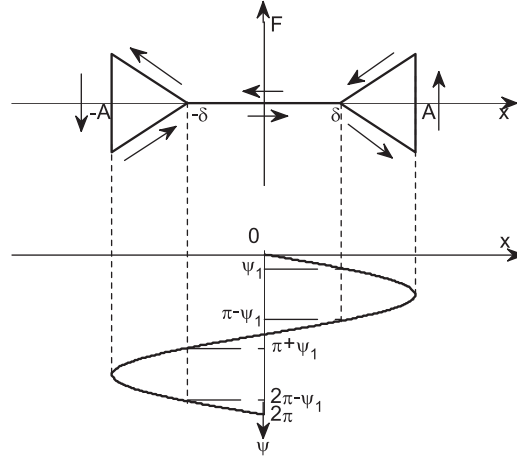


Figure 18. Nonlinear damping force.

$$\begin{aligned}
 n_p &= \frac{1}{\pi A} \int_{2\pi}^0 f_{Cnl,3}(A \sin \psi, \omega A \cos \psi) \sin \psi d\psi \\
 &= -\frac{1}{\pi A} \int_0^{2\pi} f_{Cnl,3}(A \sin \psi, \omega A \cos \psi) \sin \psi d\psi
 \end{aligned} \tag{28}$$

$$\begin{aligned}
 n_q &= -\frac{1}{\pi A} \int_{2\pi}^0 f_{Cnl,3}(A \sin \psi, \omega A \cos \psi) \cos \psi d\psi \\
 &= -\frac{1}{\pi A} \int_0^{2\pi} f_{Cnl,3}(A \sin \psi, \omega A \cos \psi) \cos \psi d\psi
 \end{aligned} \tag{29}$$

As this is a non-conservative (dissipative) force, the in phase term is expected to be zero. Defining the switching point

$$A \sin \psi_1 = \delta \tag{30}$$

Applying the definition in equations (28) and separating those regions within the integral when the gaps are either open or closed (so the k_2 is active)

$$\begin{aligned}
n_p = & -\frac{1}{\pi A} \int_0^{\psi_1} (\varepsilon|0|\operatorname{sgn}(\omega A \cos \psi)) \sin \psi d\psi \\
& -\frac{1}{\pi A} \int_{\psi_1}^{\pi-\psi_1} (\varepsilon|k_2(A \sin \psi - \delta)| \operatorname{sgn}(\omega A \cos \psi)) \sin \psi d\psi \\
& -\frac{1}{\pi A} \int_{\pi-\psi_1}^{\pi+\psi_1} (\varepsilon|0| \operatorname{sgn}(\omega A \cos \psi)) \sin \psi d\psi \\
& -\frac{1}{\pi A} \int_{\pi+\psi_1}^{2\pi-\psi_1} (\varepsilon|k_2(A \sin \psi + \delta)| \operatorname{sgn}(\omega A \cos \psi)) \sin \psi d\psi \\
& -\frac{1}{\pi A} \int_{2\pi-\psi_1}^{2\pi} (\varepsilon|0| \operatorname{sgn}(-\omega A \cos \psi)) \sin \psi d\psi
\end{aligned} \tag{31}$$

Simplifying the regions in which the force is null

$$\begin{aligned}
n_p = & \frac{1}{\pi A} \int_{\psi_1}^{\pi-\psi_1} \varepsilon k_2(A \sin \psi - \delta) \operatorname{sgn}(\omega A \cos \psi) \sin \psi d\psi \\
& -\frac{1}{\pi A} \int_{\pi+\psi_1}^{2\pi-\psi_1} -\varepsilon k_2(A \sin \psi + \delta) \operatorname{sgn}(\omega A \cos \psi) \sin \psi d\psi
\end{aligned} \tag{32}$$

The ‘signum’ function may be eliminated by casting the above equation as follows

$$n_p = -\frac{1}{\pi A} \left[\int_{\psi_1}^{\frac{\pi}{2}} \varepsilon k_2(A \sin \psi - \delta) \sin \psi d\psi + \int_{\frac{\pi}{2}}^{\pi-\psi_1} -\varepsilon k_2(A \sin \psi - \delta) \sin \psi d\psi \right. \\
\left. + \int_{\pi+\psi_1}^{\frac{3}{2}\pi} \varepsilon k_2(A \sin \psi + \delta) \sin \psi d\psi + \int_{\frac{3}{2}\pi}^{2\pi-\psi_1} -\varepsilon k_2(A \sin \psi + \delta) \sin \psi d\psi \right] \tag{33}$$

Computing the integrals, one finds that

$$n_p = 0 \tag{34}$$

The term in quadrature is computed by applying equation (29). Simplifying the region in which the integrand function is zero results in

$$\begin{aligned}
n_q = & -\frac{1}{\pi A} \int_{\psi_1}^{\pi-\psi_1} (\varepsilon k_2 (A \sin \psi - \delta) \operatorname{sgn}(\omega A \cos \psi)) \cos \psi d\psi \\
& -\frac{1}{\pi A} \int_{\pi+\psi_1}^{2\pi-\psi_1} (-\varepsilon k_2 (A \sin \psi + \delta) \operatorname{sgn}(\omega A \cos \psi)) \cos \psi d\psi
\end{aligned} \tag{35}$$

Eliminating the ‘signum’ function as before

$$n_q = -\frac{1}{\pi A} \left[\int_{\psi_1}^{\frac{\pi}{2}} \varepsilon k_2 (A \sin \psi - \delta) \cos \psi d\psi + \int_{\frac{\pi}{2}}^{\pi-\psi_1} -\varepsilon k_2 (A \sin \psi - \delta) \cos \psi d\psi \right. \\
\left. + \int_{\pi+\psi_1}^{\frac{3}{2}\pi} \varepsilon k_2 (A \sin \psi + \delta) \cos \psi d\psi + \int_{\frac{3}{2}\pi}^{2\pi-\psi_1} -\varepsilon k_2 (A \sin \psi + \delta) \cos \psi d\psi \right] \tag{36}$$

Computing all the integrals, the in-quadrature term becomes

$$n_q = -\frac{2\varepsilon k_2}{\pi} \left(1 - \frac{\delta}{A}\right)^2 \tag{37}$$

The DF for the nonlinear damping force when $A > \delta$ is

$$N_{Cnl}(\omega, a) = n_p + in_q = n_p + \frac{n_q}{\omega} s = 0 + i \left(-\frac{2\varepsilon k_2}{\pi} \left(1 - \frac{\delta}{A}\right)^2 \right) = -i \frac{2\varepsilon k_2}{\pi} \left(1 - \frac{\delta}{A}\right)^2 \tag{38}$$

The complete formulation can be written as

$$N_{Cnl}(\omega, a) = -i \frac{2\varepsilon k_2}{\pi} \left(1 - g\left(\frac{\delta}{A}\right)\right)^2 \tag{39}$$

where

$$g(\chi) = \begin{cases} -1 & \chi < -1 \\ \frac{\delta}{A} & |\chi| \leq 1 \\ 1 & \chi > 1 \end{cases}, \quad \chi = \frac{\delta}{A} \tag{40}$$